Applied Catalysis B: Environmental 242 (2019) 507–517

Contents lists available at ScienceDirect

Applied Catalysis B: Environmental

journal homepage: www.elsevier.com/locate/apcatb

Anodic electrophoretic deposition of Bi_2WO_6 thin film: high photocatalytic activity for degradation of a binary mixture

Mahboobeh Zargazi[a], Mohammad H. Entezari[a,b,*]

[a] Sonochemical Research Center
[b] Environmental Chemistry Research Center, Department of Chemistry, Faculty of Science, Ferdowsi University of Mashhad, Mashhad, Iran

ARTICLE INFO

Keywords:
Anodic electrophoretic deposition
Bi_2WO_6thin film
Single and binary mixture
Photocatalytic degradation

ABSTRACT

It is known that many thin films are able to remove pollutants. In the present work, anodic electrophoretic deposition, a low cost, one-step and flexible approach was successfully employed to prepare Bi_2WO_6 thin films. The film was fabricated from stable suspensions consisted of acetone and Bi_2WO_6 flower like nanostructures without any dispersant. The deposition was achieved on the anode at applied voltages in the range of 30–70 V using a total solid loading of 0.05-0.20 g L^{-1} under ambient condition. The kinetics and mechanism of electrophoretic deposition of Bi_2WO_6 films were studied in details. As-prepared thin films were characterized by scanning electron microscope, energy dispersive X-ray spectroscopy, atomic force microscope, X-ray diffraction, and Raman analysis. Moreover, the photocatalytic activity of thin films was evaluated through degradation of single and binary mixture of 4-cholorophenol and 4-nitrophenol as a pollutant model under natural sunlight and Xe lamp irradiation. A photocatalytic set up with fixed rotating speed was designed for degradation process. The photocatalytic activity was found to be dependent on the substrate and the film thickness. For this purpose, the effect of the film thickness was investigated on the efficiency of photocatalytic degradation in a binary mixture of pollutants. The optimum degradation was achieved by film with thickness of 627 nm.

1. Introduction

Recently, numerous studies have been focused on the synthesis of photocatalytic thin films for diverse applications from photocatalytic removal of pollutants and photoelectrochemical water splitting to solar cells. TiO_2 as a UV-active photocatalyst was used for environmental issues such as photocatalytic degradation of various toxic pollutants of air and energy storage through water splitting [1–4]. In the visible light region, anion-doping with N, C, S or cation-doping with transition metals [5], ion implantation [6] and coupling with narrow band gap semiconductors [7] are commonly used to activate TiO_2. However, these doped TiO_2 materials show low absorption of visible light and their photocatalytic activities are still very low, owing to other complicated factors. Thus the synthesis of visible light-driven photocatalysts has been major challenge from the viewpoint of the optimum use of natural sunlight. In recent years, bismuth-containing nanomaterial were found to be potentially high-active visible light photocatalysts. Consequently, several attempts have been devoted to developing bismuth-containing photocatalysts, such as $BiVO_4$, Bi_2WO_6, $Bi_4Ti_3O_{12}$ and $BiFeO_3$ [8–11]. Among them, Bi_2WO_6 has shown excellent visible–light active photocatalysts on the degradation of contaminants and oxygen evolution from water decomposition [12,13]. Bi_2WO_6 has a layered structure in which WO_6 octahedral are placed between $(Bi_2O_2)^{2+}$ layers. Electrons can migrate to the photocatalyst surface along the layered structure and lowered recombination of photogenerated electron-hole pairs by electron transferring to layered host [14,15].

These photocatalysts are usually employed in a powdered form. In a slurry state, there are some problems such as low photodegradation efficiency and low recovery of the nanoparticles which noticeably limited their applications. In order to overcome the obstacles, photocatalytic films made to adhere to the solid supports have exhibited excellent photocatalytic performance compared with powders. For instance, ZnO [16] and TiO_2 [17] films on solid supports have been developed and exhibited a large specific surface area, high porosity, and excellent photocatalytic performance compared to powdered forms. Up to the present, Bi-based films have been synthesized by several different approaches. For example, BFO films have been deposited by electrophoretic deposition on a stainless steel substrate and applied to photocatalytic degradation of organic dyes [18,19]. Other Bi-based films such as BiOX (X = Cl I) [20–23], $BiPO_4$ [24,25], $BiTiO_4$ [26,27], and

* Corresponding author at: Sonochemical Research Center, Environmental Chemistry Research Center, Department of Chemistry, Faculty of Science, Ferdowsi University of Mashhad, Mashhad, Iran.
E-mail address: entezari@um.ac.ir (M.H. Entezari).

https://doi.org/10.1016/j.apcatb.2018.09.093
Received 19 July 2018; Received in revised form 13 September 2018; Accepted 29 September 2018
Available online 03 October 2018
0926-3373/

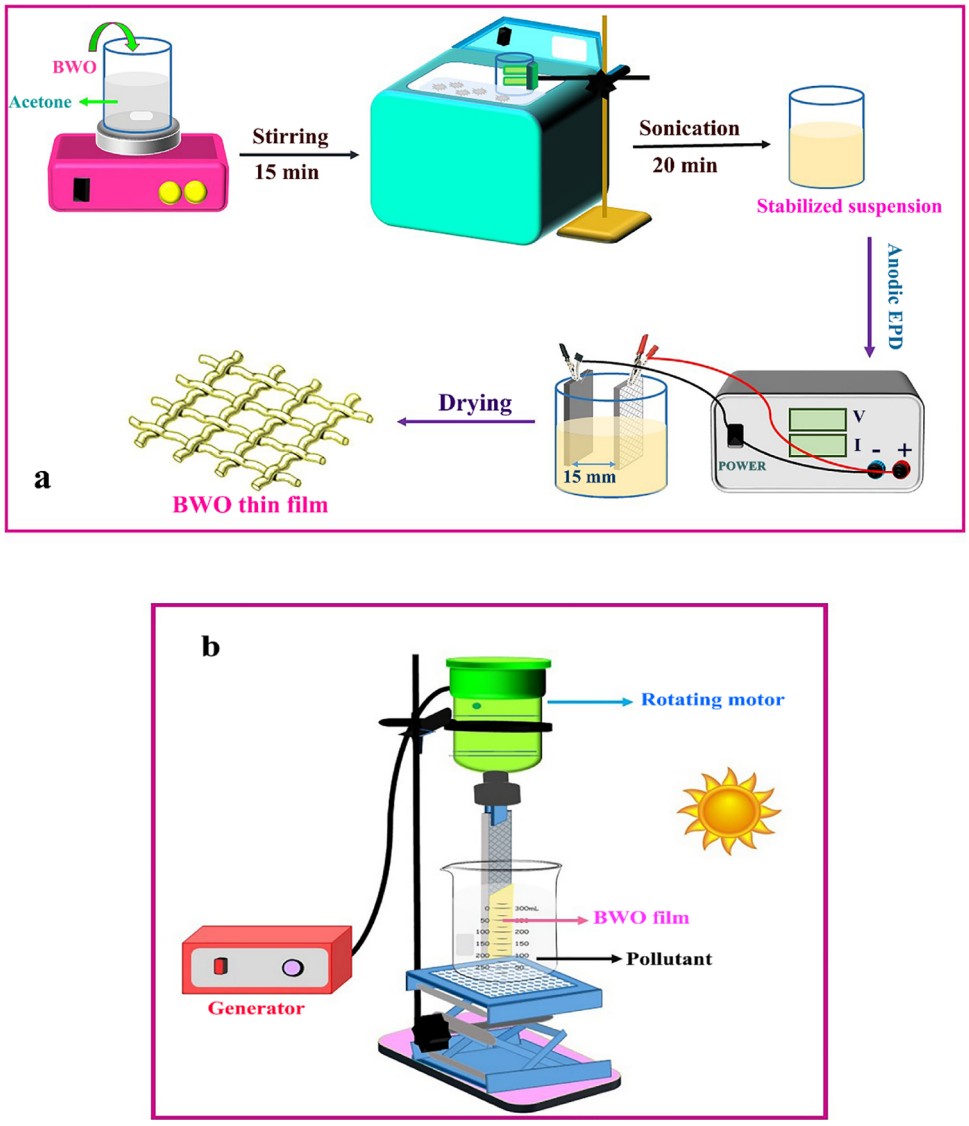

Fig. 1. Preparation process of BWO thin film (a) and schematic of photocatalytic set up (b).

Bi_2Te_3 [28] were also synthesized by various methods. These kinds of films have drawn more attention of researchers in study of visible light photocatalytic degradation of different pollutants. To the best of our knowledge, there are still no reports focused on the Bi_2WO_6 thin films of visible-light active ternary metal oxide photocatalysts. Li Wu et al. [29] described a strategy for extending the general methodology of template-directed synthesis to the formation of porous ternary metal oxides Bi_2WO_6 thin film. The photocatalytic activity of the as-prepared porous films was evaluated by the decomposition of methylene blue under visible light ($\lambda > 420$ nm) irradiation. Ratovaa et al. [30] also reported that Bi_2WO_6 films have been deposited on glass by DC reactive magnetron sputtering for photocatalytic application. Until now, there are no reports of the synthesis of Bi_2WO_6 film by electrophoretic deposition method. Electrophoretic deposition is a simple, low-cost, repeatable and controllable method for synthesis of films on different shaped substrates. Among pollutants, phenolic compounds such as 4-cholorophenol (4-CP) and 4-nitrophenol (4-NP) are widely used in various fields, leading to their increased disposal. Some of them are highly toxic and carcinogenic and can remain in the environment for long times owing to their stability and bioaccumulation. Phenol and its derivatives are the precursors or additives in variety industries such as paper, resin and dyes, and pharmaceutics. They are also used as herbicides and pesticides in agriculture. They are harmful even at low levels and produce problems in respiratory and nervous systems and also causes cancer at higher levels. Eleven phenolic compounds have been listed by USEPA as priority pollutants [31,32]. Petroleum industries produce phenolic compounds which could be polluted surface waters such as rivers and seas (Caspian, Persian Gulf) [33–35]. Among of phenolic compounds, chlorophenols and nitrophenols appear commonly in industrial effluents. A large numbers of works in the literature focused on the photocatalytic degradation of chlorophenols and nitrophenols [36–38]. Most of the studies are on the degradation of an individual organic pollutant by powder photocatalysts. 4-Cholorophenol as resisted pollutant often has inhibition effects on the degradation of other phenols, due mainly to the incompatibility of different pathways [39]. However, only a few studies have investigated the photocatalytic degradation of pollutant mixtures by photocatalytic powders [40].

In the present work, Bi_2WO_6 (BWO) thin films as efficient visible light active photocatalyst were synthesized by electrophoretic deposition (EPD) for the first time, and the growth mechanism was investigated. Effective parameters of the process such as electrical field strength, loading concentration and deposition time were also evaluated under controlled conditions. The photocatalytic activity of the as prepared thin films was estimated by the degradation of a mixture (4CP/4NP) as a pollutant model under direct sunlight and Xe lamp. The

influence of film thickness on the photocatalytic degradation was also studied and optimized.

2. Experimental section

2.1. Materials

Bismuth nitrate ($Bi(NO_3)_3.5H_2O$), sodium tungstate ($Na_2WO_4.2H_2O$), 4-nitrophenol, 4-cholorophenol and all of the solvents were purchased from Merck. All reagents were used without further purification.

2.2. Fabrication and characterization of BWO thin films

The visible light active BWO nanostructure was synthesized via ultrasonic assisted-hydrothermal approach. The preparation process was briefly as follows:

Solution A: 2 mmol Bi $(NO_3)_3.5H_2O$ was added to 20 mL deionized water and stirred for 15 min to obtain a clear solution. Solution B: 1 mmol $Na_2WO_4.2H_2O$ was dissolved in 20 ml deionized water. The container of solution A was placed to a cup horn ultrasonic system (ultrasonic processor GEX 750, 20 kHz, 750 W). Then solution B was slowly added to solution A during sonication. The resulting white suspension was transformed into a 50 mL Teflon-lined stainless steel autoclave and heated at 150 °C for 20 h. After being cooled in the autoclave to room temperature, the precipitate was washed by deionized water and ethanol several times and was dried at 80 °C for 5 h.

To obtain a stable suspension, 0.10 g L^{-1} BWO nanoparticles were dispersed in 50 mL of different solvents (water, ethanol, acetone, isopropanol, and mix of water-alcohol) under ultrasound (BRANSON bath, 40 kHz). The synthesis process of thin film was shown schematically in Fig. 1a. As prepared stabilized suspensions were utilized in the synthesis of thin film by EPD process. The BWO films were formed by anodic EPD on polished commercial stainless steel mesh substrates of 3 × 2 cm^2. Polishing of the substrate was carried out using an electrolyte containing oxalic and sulfuric acid with emerge paper (grid from 200 to 1500) and then it was immersed in ethanol and acetone for 10 min under ultrasound, respectively. A stainless steel with similar dimensions was chosen as the counter electrode, separated from the working electrode by a distance of 15 mm in the electrophoretic cell. EPD was performed under potentiostatic conditions using DC power supply (TF 102, TERCO), applying voltages from 30 to 70 V. The obtained samples were left to dry at room conditions.

The yield of deposition was determined from the weight of deposition on the surface measured by an electrical balance (Sartorius, TE 1245, d = 0.1 mg). The X-ray diffraction analysis of BWO thin film on a stainless steel mesh substrate was carried out using XRD. It was done by Explorer GNR Italia at a voltage of 40 kV and a current of 30 mA with Cu K radiation (λ = 1.5418 Å) in the 2θ range 10°–80° with scan rate of 10° /min. Raman analysis was recorded by AVANTES Sensline (AvaSpec-ULS-TEC, Poland). The morphology and thickness of BWO thin film on substrate were obtained using atomic force microscopy (AFM, Ara research, Iran) and scanning electron microscopy (SEM, LEO, Germany) with an accelerating voltage of 15 kV. Elemental analysis of BWO thin film was accomplished by energy dispersive spectrometry (EDS, Inca-350, Oxford instruments) attached to SEM. The specific surface area of samples was measured by BET method (AUTOSORB-1, Quantachrome instruments inc. USA).

2.3. Photocatalytic activity

2.3.1. Calibration of spectrophotometer for a binary mixture

It is a difficult task to calibrate the analysis of any individual pollutants in a mixture owing to the interference of one pollutant on another as shown in Fig. 2a. Due to this interference, the traditional spectrophotometric method is not able to analyze the individual

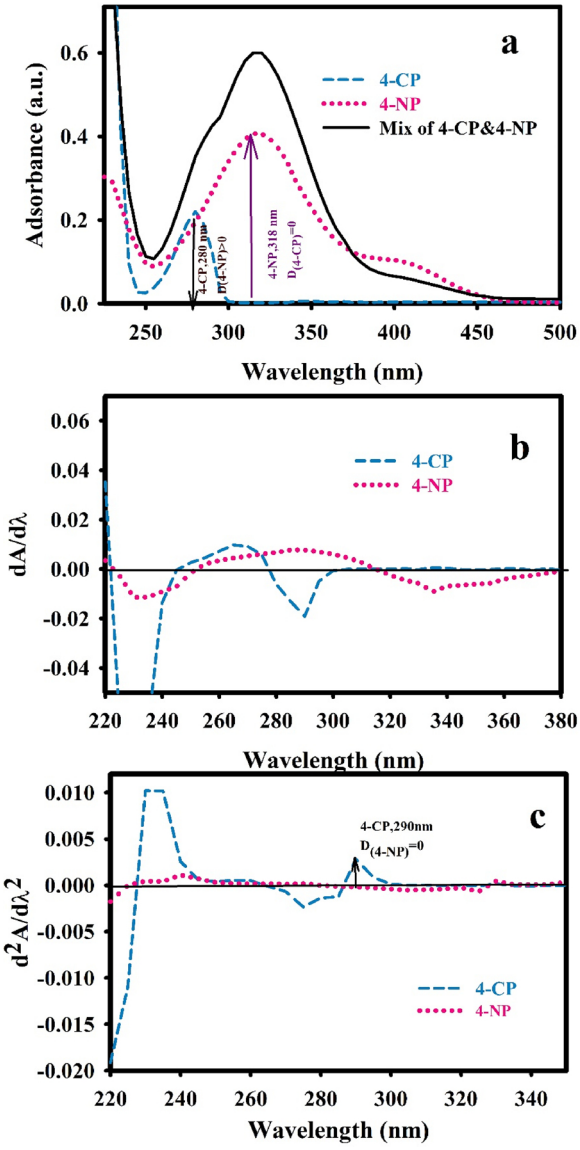

Fig. 2. Zero order UV spectra (a), first order derivative spectra (b) and second order derivative spectra (c) of 4-CP and 4-NP in single mode and binary mixture.

pollutant concentration in a binary mixture of pollutants. Here, derivative spectrophotometric technique could be used to find concentration of individual pollutant. The first (or second) derivative absorption spectrum is the first (or second) derivative of the absorbance vs wavelength. In the derivative spectrum, there is an ability to detect and to measure simultaneously spectral features of several samples with high sensitivity. The absorption spectra of individual and binary mixture of 4-CP and 4-NP are shown in Fig. 2a. Characteristic wavelength (λ_{max} = 318 nm) of 4-NP was measured in binary mixture by zero UV–vis spectroscopy because 4-CP hasn't any absorbance (D_{4CP} = 0) at this wavelength. So 4-NP can be measured from zero order UV–vis spectrum. But about measurement of 4-CP, it can be seen clearly, characteristic wavelength (λ_{max} = 280 nm) was completely overlapped by 4-NP ($D_{4\text{-}NP} \neq 0$). This behavior causes interference in the measurement of 4-CP in the binary solution. To overcome this interference, derivative method from UV–vis spectra was used. Initially, first order derivative of absorbance vs wavelength was calculated and curve was shown in Fig. 2b, but it can be seen from the curve that there still interference between 4-CP and 4-NP. At the end, second derivative of absorbance vs wavelength calculated for binary system as shown

Fig. 2c. It can be found that the interference of 4-NP was removed. Therefore, for the binary solution of 4-CP and 4-NP pollutants, the concentration of 4-CP could be determined at 290 nm in the presence of 4-NP from the second order derivative of absorbance vs wavelength which the absorbance of 4-NP is found to be zero at 290 nm.

2.3.2. Photocatalytic degradation of binary pollutants

The photocatalytic activities of BWO thin film on mesh substrate were evaluated through the degradation of 10 ppm (5 ppm 4-CP and 5 ppm 4-NP) of dual pollutants in water. Prior to irradiation, films (effective surface area = 3 cm^2) were immersed in pollutants solution and placed in the dark for 2 h to gain an adsorption-desorption equilibrium. In a typical photocatalytic experiment, the immobilized BWO thin film was hung and rotated (100 rpm) under direct natural sunlight in the edge of window during May 2018 in Mashhad, Iran between 11.00 a.m. and 13.30 pm (GPS coordinates: N = 36°18041.600, E = 59°31054.200) in a cylindrical glass reactor with an effective volume of 30 mL pollutant solution (see Fig. 1b). The samples of pollutant model were taken out and determined the concentration of pollutants at t time (C_t) relative to initial concentration (C_0) using a UV–vis spectrometer (UV spectrophotometer UNICO 2008).

For comparison, BWO nanoparticles were deposited on the non-conductive glass surface (depicted by BWO/glass) via dip coating, then photocatalytic activities of BWO/glass and BWO nano-powders were also evaluated under natural sunlight. Furthermore, the substrate without photocatalyst was used for photolysis experiments of binary and single modes of pollutants. In comparison studies, photocatalytic degradation of a binary and single modes of pollutants were also investigated under Xe lamp (400 W, HID, XT-400-E40) with cut of filter UV 400 (3 mm, Scott) as an artificial visible light source (spectral distribution graph of Xe lamp [41]). The mineralization of pollutants was assessed via the decrease in chemical oxygen demand (COD) of the pollutant solution. The COD value was measured on the basis of the standard dichromate titration method [42].

3. Results and discussion

3.1. Role of solvent in EPD

In EPD process, the solvent has an important role in sustainability of suspensions. A proper deposition was achieved by a solvent with a dielectric constant in the range of 12-25. A very low dielectric constant causes deposition to fail because it could not produce adequate free ions (free ions have an effective role in stability of suspensions). Whereas a high dielectric constant leads to increase conductivity and decrease electrophoretic mobility of nanoparticles and finally EPD failed. For a successful EPD process, the solvents must have relatively high dielectric constants, low viscosity, and low conductivity. The electrophoretic mobility of the nanoparticles (μ) was affected by physical properties of solvents according to the Huckel Eq. (1).

$$\mu = \varepsilon\xi/6\pi\eta \quad (1)$$

Where ε, ζ and η were dielectric constant, zeta potential and viscosity of suspensions, respectively. According to Fig. 3, an optimal and uniform deposition was obtained from the suspension containing nanoparticles and acetone as solvent without additive as dispersant. Acetone has proper properties for EPD process compared with other solvents. The deposition yield was low for the other solvents. Table 1 shows the physical properties such as viscosity and relative dielectric constant for different solvents.

3.2. Phase structure and morphology analysis of as-prepared thin films

Fig. 4a presents the XRD pattern of a sample. All of the diffraction peaks of the film were assigned to BWO compound and it confirmed the formation of orthorhombic BWO crystal phase (ICCD data base. No. 04-001-8551) with space group Pca21 and lattice parameters a = 5.4500 Å, b = 16.4000 Å and c = 5.4500 Å without impurity. Raman spectra of the as-prepared sample is shown in Fig. 4b. The peaks in the range 600–1000 cm^{-1} are related to the stretching of the W—O bands, according to the report by Crane et al. [43]. In detail, the bands at 790 and 820 cm^{-1} are assigned to the antisymmetric and symmetric Ag modes of terminal O–W–O groups. The band at 310 cm^{-1} can be assigned to translational modes involving simultaneous motions of Bi^{3+} and WO_6^{-6}. The peak at 700 cm^{-1} is interpreted as an antisymmetric bridging mode, associated with the tungstate chain.

Fig. 5a shows a 2D AFM topography of the film and the structure of BWO can be clearly observed in the film. The amplitude map (Fig. 5b) shows the organization of the flower structure parallel to the substrate. Moreover, the profile of the topography (black line in Fig. 5a) shows a local roughness < 10 nm in Fig. 5c. It also confirms the orientation of the flower structure parallel to the substrate. The 3D image in Fig. 5d, shows the thickness of the film that is 627 nm. The SEM image (see Fig. 6(a–c)) exhibits a relatively even distribution of obtained films, which was covered the substrate uniformly and continuously.

Fig. 6(d–f) corresponds to the elemental map. The uniformity of obtained coatings is clearly seen in the distribution diagrams of all elements of Bi, W and O. Fig. 6g shows the EDS results and the spectrum for the film surface displays the expected elemental signals related to the composition of the coating material with a relatively intense peak of Bi, W, O and Au. Here, Bi, O, and W are seen as the main peaks, which are evidence of the successful use of EPD to synthesize of BWO nano coatings. The Au peak was related to deposition of Au thin layer on the film surface at the pretreatment step for SEM studies.

3.3. Dynamic studies

Hamaker [44] has explored the correlation between the deposition yields with different effective parameters during EPD process. Hamaker's law ascribes the deposit yield (w) to the electric field strength (E), the electrophoretic mobility (μ), the surface area of the electrode (A), and nanoparticles concentration in the suspension (C) through the following equation:

$$w = \int_{t1}^{t2} \mu.\ A.\ C.\ E\ dt \quad (2)$$

In this study, the kinetics of EPD of nano-BWO coatings was evaluated under different electrical field strengths (E = V/d) by changes the applied voltages (V) of 30, 40, 50, 60 and 70 V at fixed distance between two electrodes (d), and the nanoparticles concentrations ranging from 0.05 to 0.20 g L^{-1}. At electrical fields created by voltages below 30 V, no film was obtained due to the high resistance of acetone. To overcome acetone resistance, higher electrical fields were used to force nanoparticles move to anode. In Fig. 1S (a–d) in supplementary material, as expected, the deposition yield has a direct relation with deposition time. The variation tendency of deposition under various applied electrical field was similar together. Comparison of different graphs in Fig. 1S in supplementary material, confirmed that the yield of deposition increases with increasing of applied field strength at the same deposition time. In addition, by increasing the nanoparticle's concentration in the suspension, the deposited yield was also increased. Fig. 2S (a–d) in supplementary material shows the deposited velocity (R) as a function of applied field strength and deposition time during EPD of nano-BWO coatings. The R (mg min^{-1} cm^{-2}) can be calculated by the following equation:

$$R = \frac{m2-m1}{A\Delta t} \quad (3)$$

where m_2, m_1, A, and Δ*t* are the deposited mass at times of t_2 and t_1, deposition area (2 cm^2), and time interval (t_2-t_1; $t_2 > t_1$), respectively.

For a fixed field strength, the deposition velocity of BWO thin film was decreased with increasing the interval deposition time. However,

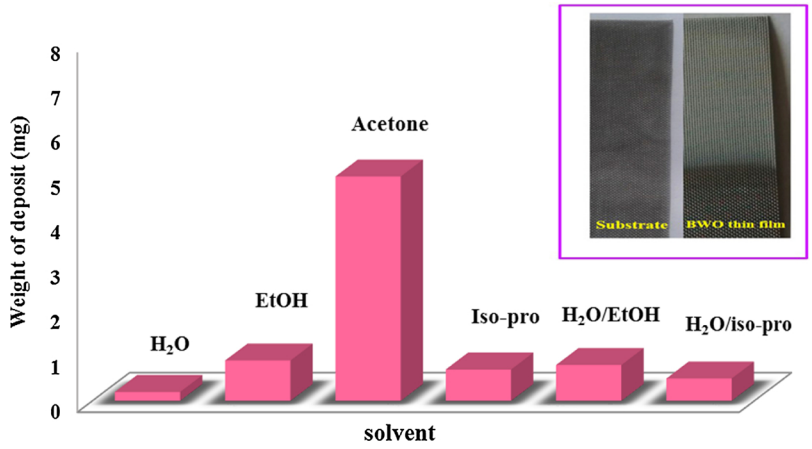

Fig. 3. The weight of deposition was measured in various solvents. Stainless steel mesh without film and with BWO film obtained in acetone as a solvent (inset).

Table 1
Physical properties of solvents used in EPD process.

Solvents	Viscosity (cP) = 10^{-3} Nsm^{-2}	Relative dielectric constant
Acetone	0.3087	20.70
Ethanol	1.088	24.55
Iso-propanol	2.043	19.92
n-Butanol	2.580	17.51
H_2O	1.000	78.54

when the field strength changes from 30 to 70 V, the deposition velocity increases accordingly (linear relation), which is mainly due to intensifying driving force in all samples. Actually, higher field strength and longer deposition time lead to increase of deposition yields [45,46]. Different correlations were observed between the deposition weight and deposition time based on Fig. 3S (a–e) in supplementary material. At short periods of time (from 0 to t_c (critical transition time), a linear relation was obtained between deposition weight and deposition time in the loading concentration of 0.20 g L^{-1}. At a primary stage of EPD ($t < t_c$), the nanoparticles participate in deposition process can be provided from optimal suspensions, resulting in the high fitted degree (R^2 close to 1). The slope varies from 2.3 at 30 V to 4.7 at 70 V, which the increasing migration rate of charged nanoparticles was led to an increasing in slope. On the other hand, at longer deposition time ($t > t_c$), the deposition mass exhibits a parabolic relation with the deposition time, which is principally related to the following combined factors, (i) the decrease of suspension resistance (high conductivity), (ii) the increase of the film resistance and (iii) change of sedimentation and flocculation rate of nanoparticles [47–49]. Additionally, the curves with different time periods have been well fitted by corresponding relations ($R^2 \geq 0.995$). Fig. 3Sf in supplementary material indicates the relationship between deposited weight and field strength. For a fixed loading concentration (0.05, 0.10, 0.15 or 0.20 g L^{-1}), it is established that the deposition weight increased linearly with increasing field strength. The results of the fitting can be found in Fig. 3Sf in supplementary material. The film thickness was calculated under applied field strength in the voltage range of 30–70 V by the following equation.

$$\rho = {}^{m}/_{A.\,d} \quad (4)$$

where ρ, m, A and d are the density of BWO (0.98 g/L), deposition weight, surface area and thickness of BWO film, respectively. Based on the above results, the weight of deposition was increased by increasing of applied field strength and led to increase of the film thickness at a constant loading concentration. According to Fig. 7, the film thickness varied from several nanometers (85 nm) to micrometers (3.8 μm) under various loading concentration. At higher loading concentration such as 0.20 g L^{-1}, it can be found that film thickness was significantly increased due to the existence of more particles in suspension which increased the migration to the electrode surface in comparison with low loading concentrations.

3.4. Photocatalytic studies

Fig. 8a shows the pollutant degradation of a binary mixture (4-CP and 4-NP) and single of each pollutant under similar experimental

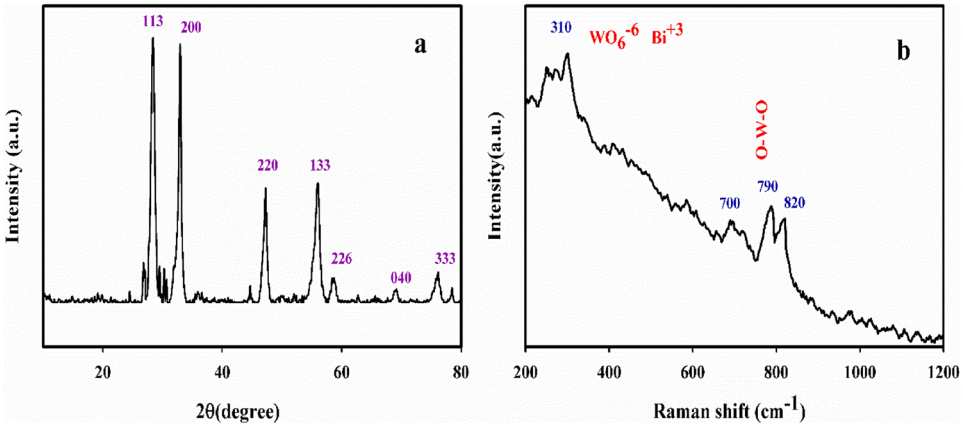

Fig. 4. X-ray diffraction pattern (a) and Raman spectrum (b) of nano BWO coatings obtained from EPD.

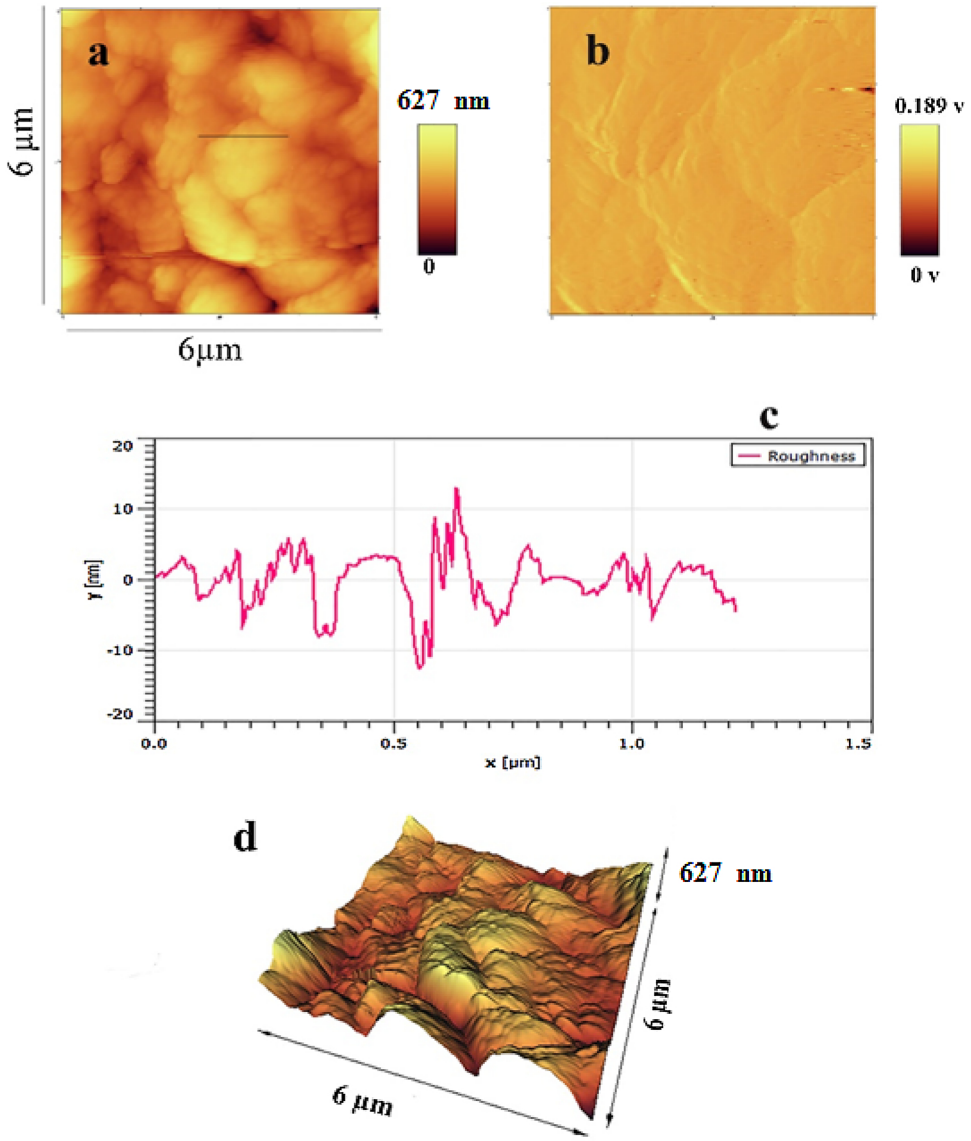

Fig. 5. Topology (a), amplitude (b), 3D (d) AFM images (6 µm × 6 µm), and roughness analysis (c) of nano-BWO coatings.

conditions. The photocatalytic degradation of binary mixture and single modes were done at the same concentration. The pH of solution in single cases and in binary mixture were approximately the same. The best results were obtained for BWO film with thickness 627 nm which synthesized by C = 0.15 g L^{-1}, V = 50 V and t = 3 min. In dark, the adsorption of binary mixture and single modes of 4-NP and 4-CP on the BWO film were 40%, 17% and 23%, respectively. As can be seen, the binary mixture was degraded in shorter time compared with single modes. Therefore, the photocatalytic efficiency can be affected by co-existence of pollutant molecules through the adsorption of each other on the photocatalyst surface. 4-CP and 4-NP in single modes have shown high resistance against photocatalytic degradation in comparison with binary mixture. The degradation pattern of binary mixture (sum of concentration of 4-NP, 4-CP is 10 mgL^{-1} (1:1)) and single modes (10 mgL^{-1}) are shown by UV–vis absorbance spectrum of samples taken in different interval times (Fig. 8b-d). Photocatalytic efficiency under Xe lamp was shown in Fig. 4S in supplementary material. The results suggested that the photocatalytic degradation under natural sunlight was slightly more than Xe lamp as the light source. On the other hand, photolysis of pollutants was investigated with substrate without film. It is confirmed that (Fig. 4S in supplementary material), there is no difference between dark and light.

The photocatalytic degradation of binary mixture was compared by nano-BWO coatings on conductive and nonconductive substrates and BWO powder as the photocatalyst under direct sunlight irradiation (Fig. 9a). The removal efficiency of pollutants was obtained from the ratio of the residual absorption intensity (C_t) to the initial intensity of the pollutant solution (C_0). The thin film on the conductive substrate (depicted by BWO/SS mesh) demonstrates higher photocatalytic activity compared with one nonconductive substrate (BWO/glass). In slurry state, the photocatalytic activity was lower than BWO/SS mesh and higher than BWO/glass sample. In thin film immobilized on the conductive substrate, although the surface area (5.96 $m^2 g^{-1}$) was reduced due to the presence of powder on the surface, but degradation rate increased which is related to the substrate effect in separation of hole-electrons, furthermore slurry problems vanished. In nonconductive substrate (BWO/glass), as seen in Fig. 9a, the photocatalytic degradation efficiency reduced due to lower surface area of photocatalyst (0.94 $m^2 g^{-1}$) as a thin film on glass than the free powder form (15.78 $m^2 g^{-1}$). Surface area of all samples was demonstrated in Fig. 5S in supplementary material which obtained from N_2 adsorption-desorption isotherm. It is noticed that the BWO/SS mesh film was completely degraded pollutants in 140 min but at the same time, the BWO powder and BWO/glass film was removed about 40% and 24%,

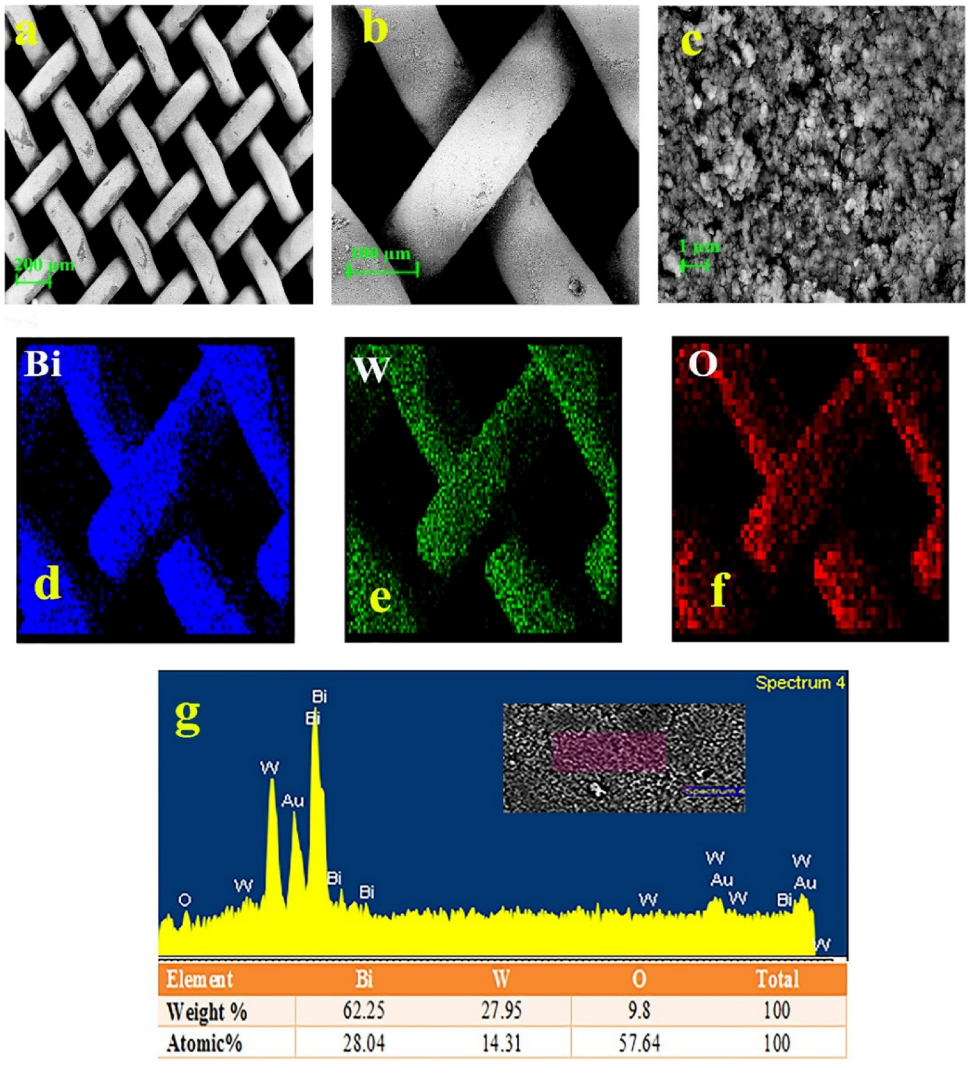

Element	Bi	W	O	Total
Weight %	62.25	27.95	9.8	100
Atomic%	28.04	14.31	57.64	100

Fig. 6. SEM images of nano-BWO coatings (a–c), the images with elemental maps of Bi (d), W (e), O (f), and EDS spectra of BWO coating (g) obtained from EPD.

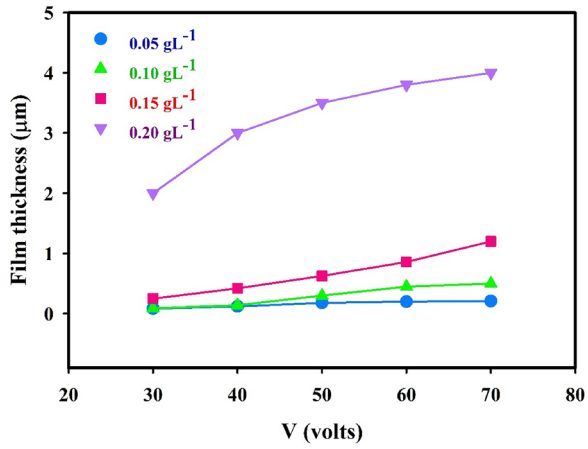

Fig. 7. Thickness of BWO film versus applied electrical field in various loading concentrations at optimal deposition time (3 min).

respectively. Moreover, kinetic linear simulation curves of photocatalytic degradation of single and binary mixture are inserted in Fig. 9b. In low reactant concentration, the following pseudo first-order kinetics model can be used:

$$-\ln(C_t/C_0) = k_{ap}t \quad (5)$$

The apparent rate constant (k_{ap}) was obtained from plotting –Ln (C_t/C_0) vs the reaction time (t). Fig. 9b shows the rate of photocatalyst reactions in binary and single modes for each pollutant. Results indicated that binary pollutants have higher degradation rates compared to single modes. Herein, the rate constants for a binary mixture and single modes of 4-CP and 4-NP were 0.027, 0.011 and 0.014, respectively. These results suggested that the degradation rate of a binary mixture was almost twice of single modes.

Fig. 9c shows the COD reduction of binary mixture of pollutants in the presence of BWO/ SS mesh as a photocatalyst. Rate of COD reduction was lower than rate of photocatalytic degradation due to generation of byproducts from photodegradation of pollutants which disappeared at longer time of illumination. The lifetime of a photocatalyst is an important parameter in a photocatalytic process. A photocatalyst is good and cost-effective when it can be used for a long period of time without lowering of performance [50]. Herein, the prepared thin film was applied for degradation of binary mixture of pollutants in several times. After using in each time, the thin film was rinsed, dried and reused in fresh pollutant solution. Fig. 9d demonstrated the durability of the synthesized thin film after uses in 5 cycles.

The proposed mechanism for the photocatalytic degradation was shown in Fig. 10. It is well known that when semiconductor materials were illuminated by a proper light, the photogenerated pair of hole-

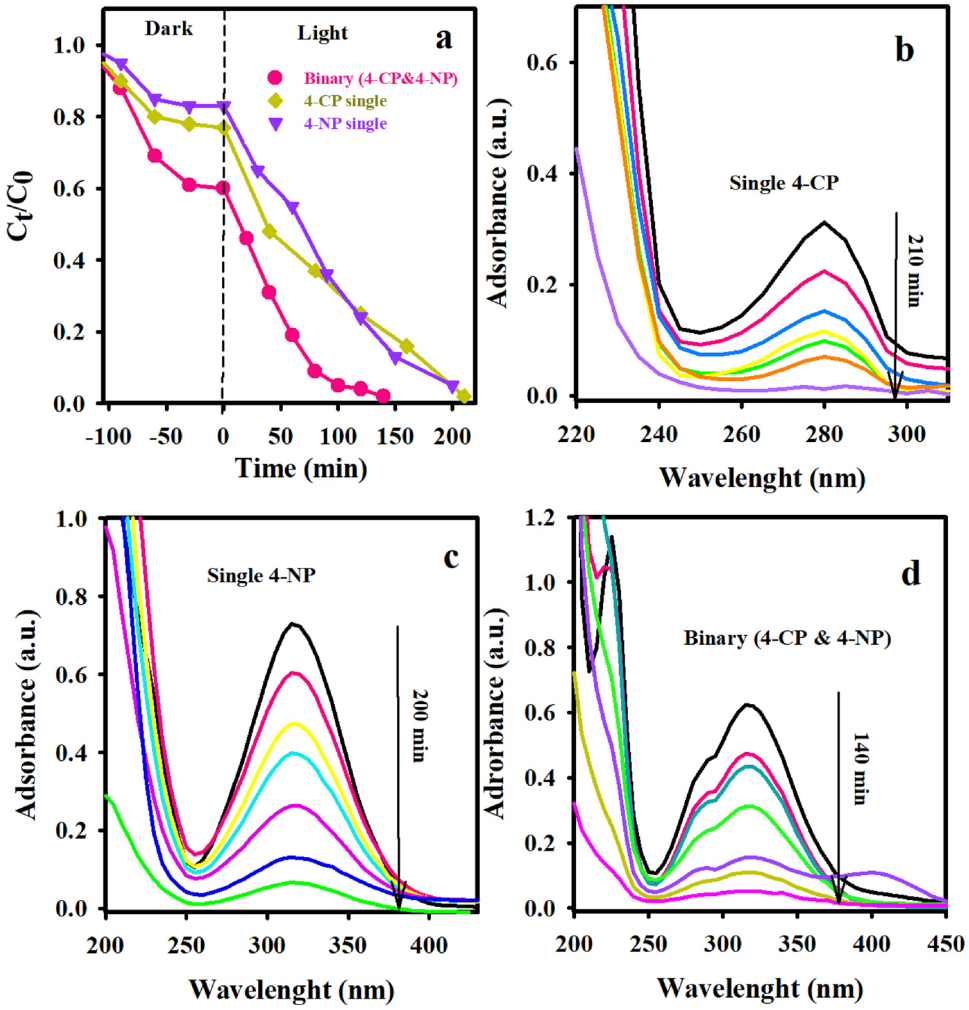

Fig. 8. Degradation of single and a binary mixture of 4-CP and 4-NP under sunlight irradiation with the nano-BWO coatings (a), UV–Vis spectra changes of two single pollutants and a mixture of them with BWO thin film at different interval times of irradiation $[4\text{-CP}]_0$: 10 mg/L (b), $[4\ NP]_0$: 10 mg/L (c), and binary mixture of $[4\text{-CP}]_0$: 5 mg/L and [4-NP]0: 5 mg/L (d).

electron on the surface can be rapidly recombined together due to its very short lifetime. Therefore, the separation of charged carriers was played a significant role in photocatalytic activity of semiconductors. Hence, the conductive substrates such as stainless steel mesh can reduce the recombination of produced active species through moving electrons to the conductive substrate. The remained electrons in conduction bands cannot interact with adsorbed oxygen and produce hydroxyl radicals due to low energy of conduction band. The transferred electrons to the substrate could be contributed in formation of hydroxyl radicals. In addition, the thin film interacted with adsorbed water can produce hydroxyl radicals because photoholes (E_{VB} = 3 eV) has level with enough energy for oxidation water ($E_{(H2O/OH^{\circ})}$ = 2.3 eV). Hence, based on proposed mechanism, high production of hydroxyl radicals in BWO film case efficiently contribute in pollutants oxidation process.

3.4.1. Thickness and performance of BWO film

In immobilized photocatalyst cases, the thickness of the film plays an important role in efficiency of photocatalytic process. The thickness of film was affected by loading concentration and applied electrical field. As mentioned in dynamic studies, at fixed loading concentration, the thickness of film was increased by increasing the applied electrical field. Based on Fig. 11, with increasing the film thickness, the efficiency of photocatalytic degradation increases too. But, the increases were continued until certain thickness (critical thickness). Increasing above critical thickness led to lowering of photocatalytic efficiency process due to decrease of the substrate effect in photocatalytic process (direct relation switched to parabolic relation). Indeed, the increase of film thickness leads to enhancing of film resistance, prolonging the electron transport routs and increasing the recombination rate of photoelectrons and holes. The best efficiency of degradation was achieved in film thickness of 627 nm.

For performance studies, the prepared film was compared with some synthesized films for degradation of pollutants (see Table 2). ZnO and TiO_2 thin films were activated by UV light that contained only 4% of solar energy. On the other hand, the organic pollutants were removed in longer times. Even, modifying these films with other elements could not improve their performances. Furthermore, thin films used for mixture of 4-NP and 4-CP has not been yet reported. Bismuth compounds such as $BiFeO_3$, Bi_2MoO_6 and Bi_2WO_6 were activated by visible light that forms a major part of the sunlight. BWO thin films synthesized by techniques such as spin coating and DC magnetron used for degradation of MB. In the present work, BWO thin film was synthesized by novel EPD method from acetone as a low cost and available solvent on the commercial substrate (stainless steel mesh with high surface area).

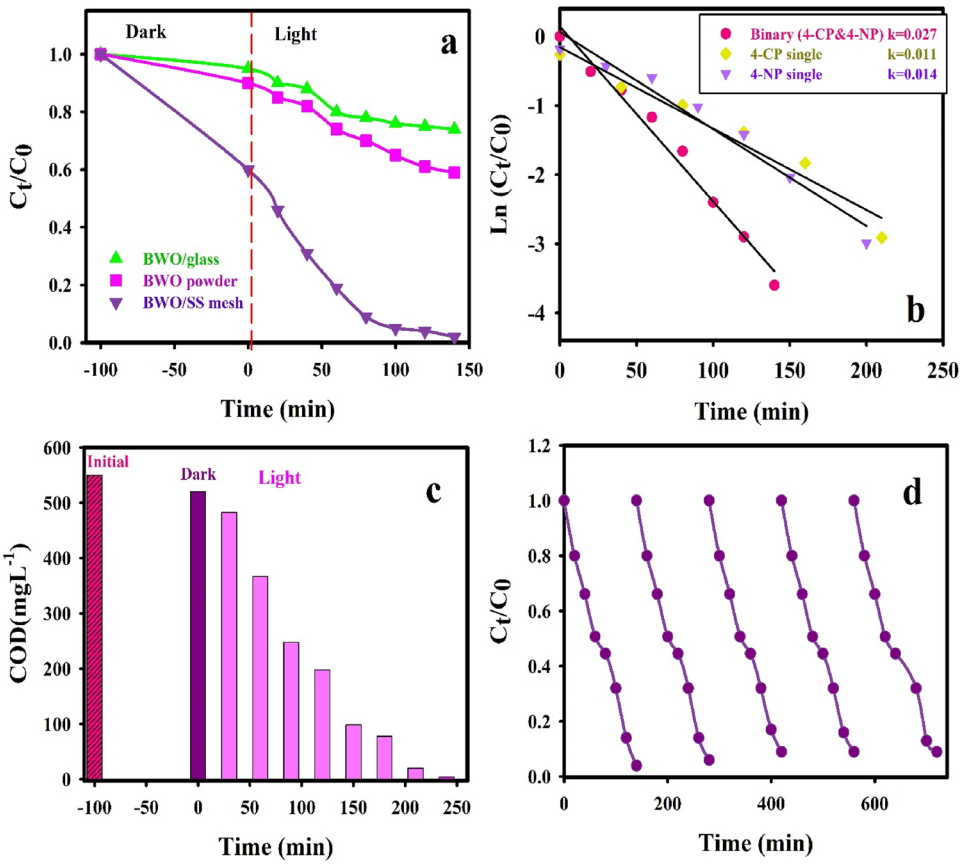

Fig. 9. Photocatalytic degradation of a binary mixture by various BWO films and powder (a), kinetic linear simulation curves of photocatalytic degradation of pollutant models at various modes (b), mineralization efficiency (COD) of pollutant model by nano-BWO coatings (c), and cycling runs in the photocatalytic degradation of pollutant model (d).

EPD technique is a simple, repeatable and controllable method in comparison with DC magnetron, RF, PLD, LPD methods. In addition, the synthesized film showed a high performance in degradation mixture of phenolic compounds in a short time.

4. Conclusion

In this work, BWO thin film was obtained from a reproducible and simple electrophoretic deposition on stainless steel mesh for the first time. Acetone as solvent has best properties, low cost and available for EPD process. Furthermore, no dispersant or additive was used to gain the stabilized suspensions. Dynamic studies of EPD process have been carried out by regulation field strength and deposition time in different concentration of BWO from 0.05–0.20 g L^{-1}. BWO films with different thicknesses were obtained in the range of 85 nm–3.8 μm. Film thickness can be dependent to some parameters such as loading concentration of BWO and applied electrical field strength. The photocatalytic activity of prepared films has been investigated for degradation of single and binary mixture of pollutants (4-NP and 4-CP) with fix rotation speed under natural sunlight irradiation. Binary mixture was demonstrated higher efficiency in degradation than single modes due to positive effect of co-existence of pollutants molecules on their adsorption behaviors.

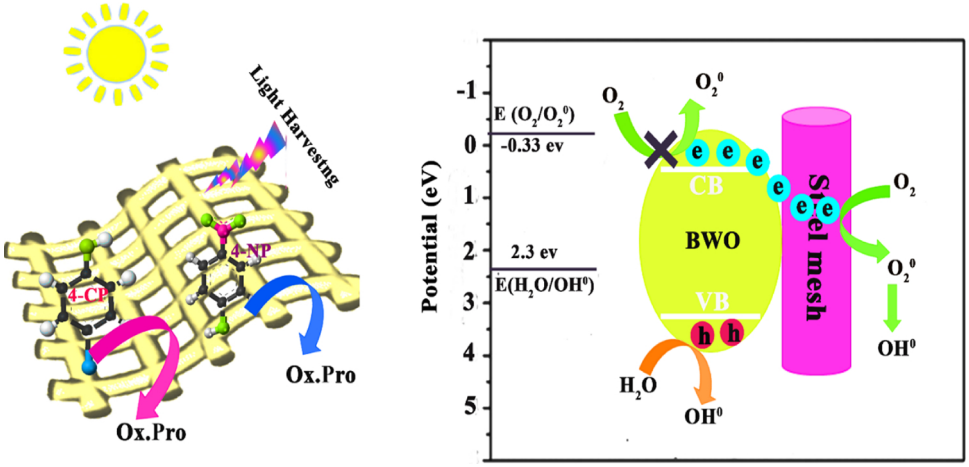

Fig. 10. Proposed mechanism for photocatalytic activity of BWO coating under sunlight irradiation.

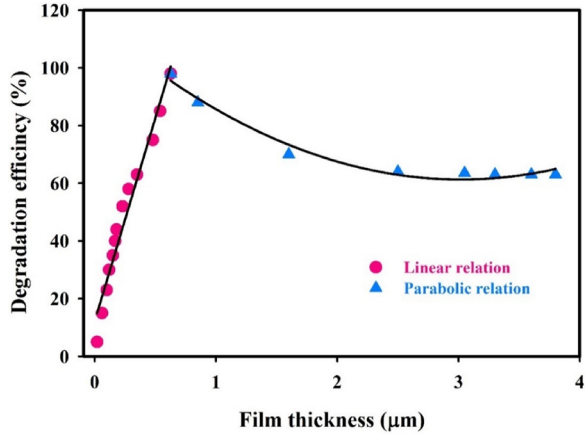

Fig. 11. Degradation efficiency of binary mixture by BWO film with different thickness ranging from nanometers to micrometers.

Table 2
Examples of synthesized film prepared by various techniques for degradation of pollutants until now.

Film	Method/Substrate	Performance	Ref
$BiFeO_3$	EPD, SS	MB,6 h,60%,visible	[18]
Bi_2MoO_6	DC reactive magnetron sputtering, glass	RhB,MB,1 h,visible	[51]
Bi_2O_3	EPD, Ni	RhB,2 h,visible	[52]
Bi_2WO_6	Spin coating, ITO	MB,5 h,visible	[29]
Bi_2WO_6	DC magnetron, glass	MB,1 h,visible	[30]
TiO_2	Glass, spin coating	MB, 4 h, visible	[17]
TiO_2-Cu	Dip coating,FTO	4-CP, 3 h, 45%, visible	[53]
TiO_2-Cu	Mechanical coating, Al ball	MB, 10 h, UV	[54]
TiO_2-N	DC magnetron, Si	MB, 40 min, 40%, visible	[55]
TiO_2/SiO_2-Cr	Dip coating, glass	MO, 180 min,70%, visible	[56]
TiO_2/ZnO/CdS	Layer by layer, Ti/TiO_2	Alzarin, 3 h, UV	[57]
TiO_2/ZnO	Spin coating	Orange II, 3 h, UV	[58]
ZnO	RF sputtering, glass	2-CP, 180 min,UV	[59]
ZnO	Spray pyrolysis deposition, FTO	MO, 3 h,UV	[60]
ZnO	Spray pyrolysis, glass	MB,4 h, Visible	[61]
ZnO/Fe_2O_3	LPD, FTO	Mix (Cu^{+2},4CP),3 h,60%, visible	[62]
Bi_2WO_6	EPD, SS mesh	Mix(4NP,4CP),140 min, visible	Present work

The highest photocatalytic efficiency was achieved by film thickness of 627 nm. Moreover, the thin film was stable in photocatalytic process even after five consecutive cycles.

Acknowledgement

The support of Ferdowsi University of Mashhad (Research and Technology) for this work (3/39052) is appreciated.

Appendix A. Supplementary data

Supplementary material related to this article can be found, in the online version, at doi:https://doi.org/10.1016/j.apcatb.2018.09.093.

References

[1] A. Fujishima, K. Honda, Electrochemical photolysis of water at a semiconductor electrode, Nature 238 (1972) 37–38.
[2] M. Ni, M.K.H. Leung, D.Y.C. Leung, K. Sumathy, A review and recent developments in photocatalytic water-splitting using TiO2for hydrogen production, Renew. Sustain. Energy Rev. 11 (2007) 401–425.
[3] S.G. Kumar, L.G. Devi, Review on modified TiO 2 photocatalysis under UV / Visible light : selected results and related mechanisms on interfacial charge carrier transfer dynamics, Phys. Chem. A 115 (2011) 13211–13241.
[4] P. Szymanski, M.A. El-Sayed, Some recent developments in photoelectrochemical water splitting using nanostructured TiO2: a short review, Theor. Chem. Acc. 131 (2012) 1202–1214.
[5] D. Ma, Y. Xin, M. Gao, J. Wu, Fabrication and photocatalytic properties of cationic and anionic S-doped TiO2nanofibers by electrospinning, Appl. Catal. B Environ. 147 (2014) 49–57.
[6] G. Impellizzeri, V. Scuderi, L. Romano, E. Napolitani, R. Sanz, R. Carles, V. Privitera, C Ion-implanted TiO2 thin film for photocatalytic application, J. Appl. Phys. 117 (2015) 10–13 105308.
[7] M.T. Uddin, O. Babot, L. Thomas, C. Olivier, M. Redaelli, M. D'Arienzo, F. Morazzoni, W. Jaegermann, N. Rockstroh, H. Junge, T. Toupance, New Insights into the Photocatalytic Properties of RuO_2 /TiO_2 Mesoporous Heterostructures for Hydrogen Production and Organic Pollutant Photodecomposition, J. Phys. Chem. C 119 (2015) 7006–7015.
[8] H. Fan, T. Jiang, H. Li, D. Wang, L. Wang, J. Zhai, D. He, P. Wang, T. Xie, Effect of BiVO4crystalline phases on the photoinduced carriers behavior and photocatalytic activity, J. Phys. Chem. C. 116 (2012) 2425–2430.
[9] X.-F. Cao, L. Zhang, X.-T. Chen, Z.-L. Xue, Microwave-assisted solution-phase preparation of flower-like Bi_2WO_6 and its visible-light-driven photocatalytic properties, CrystEngComm 13 (2011) 306–311.
[10] M.T. Buscaglia, M. Sennour, V. Buscaglia, C. Bottino, V. Kalyani, P. Nanni, Formation of Bi4Ti3O12 one-dimensional structures by solid-state reactive diffusion. from core-shell templates to nanorods and nanotubes, Cryst. Growth Des. 11 (2011) 1394–1401.
[11] S. Li, Y.-H. Lin, B.-P. Zhang, Y. Wang, C.-W. Nan, Controlled fabrication of BiFeO 3 uniform microcrystals and their magnetic and photocatalytic behaviors, J. Phys. Chem. C. 114 (2010) 2903–2908.
[12] Y.M.F. Wang, X.F. Qin, Y.F. Meng, Z.L. Guo, L.X. Yang, D. Chen, X. Jiao, M. Zhang, Hydrothermal synthesis and characterization of, Mater. Res. Bull. 35 (2000) 2101–2108.
[13] L. Zhang, W. Wang, L. Zhou, H. Xu, Bi2WO6 Nano- and microstructures: shape control and associated visible-light-driven photocatalytic activities, Small. 3 (2007) 1618–1625.
[14] J. Tang, Z. Zou, J. Ye, Photocatalytic decomposition of organic contaminants by Bi_2WO_6 under visible light irradiation, Catal. Letters 92 (2004) 53–56.
[15] H. Fu, C. Pan, L. Zhang, Y. Zhu, Synthesis, characterization and photocatalytic properties of nanosized Bi2WO6, PbWO4and ZnWO4catalysts, Mater. Res. Bull. 42 (2007) 696–706.
[16] J. Moore, R. Louder, C. Thompson, Photocatalytic activity and stability of porous polycrystalline zno thin-films grown via a two-step thermal oxidation process, Coatings 4 (2014) 651–669.
[17] D. Komaraiah, P. Madhukar, Y. Vijayakumar, M.V. Ramana Reddy, R. Sayanna, Photocatalytic degradation study of methylene blue by brookite TiO2thin film under visible light irradiation, Mater. Today Proc. 3 (2016) 3770–3778.
[18] C. Ponzoni, R. Rosa, M. Cannio, V. Buscaglia, E. Finocchio, P. Nanni, C. Leonelli, Electrophoretic deposition of multiferroic BiFeO3 sub-micrometric particles from stabilized suspensions, J. Eur. Ceram. Soc. 33 (2013) 1325–1333.
[19] M. Zargazi, M.H. Entezari, BFO thin film on the stainless steel mesh by anodic EPD: A visible light photocatalyst for degradation of Rhodamin B, J. Photochem. Photobiol. A: Chem. 365 (2018) 185–198.
[20] S.H.I. Zhu-qing, W. Yan, F.A.N. Cai-mei, W. Yun-fang, D. Guang-yue, Preparation and photocatalytic activity of BiOCl catalyst, Trans. Nonferrous Met. Soc. China. 21 (2011) 2254–2258.
[21] E.L. Cuellar, J.O. Cortés, A.M. Cruz, A.G. Loera, U.O. Méndez, Thin films of BiOCl were prepared by a sequential evaporation process in a Thermal, Thin Solid Films 659 (2018) 57–63.
[22] L. Ye, J. Chen, L. Tian, J. Liu, T. Peng, K. Deng, L. Zan, BiOI thin film via chemical vapor transport: Photocatalytic activity, durability, selectivity and mechanism, Appl. Catal. B Environ. (2013) 130–131.
[23] Y. Wang, Y. Long, D. Zhang, Facile in Situ Growth of High Strong BiOI Network Films on Metal Wire Meshes with Photocatalytic Activity, ACS Sustain. Chem. Eng. 5 (2017) 2454–2462.
[24] Z. Qiu, T. Zeng, K. Ye, X. Yu, Y. Zhu, Y. Zhang, Electrochemical Synthesis of Photoelectrocatalytic Thin Films of Hexagonal BiPO 4 Nanorods, J. Electrochem. Soc. 163 (2016) 18–23.
[25] T. Zeng, X. Yu, K. Ye, Z. Qiu, Y. Zhu, X. Yu, K. Ye, Z. Qiu, Y. Zhu, Y. Zhang, Inorg. BiPO4 film on ITO substrates for photoelectrocatalytic degradation, Chem. Commun. (Camb.) 58 (2015) 39–42.
[26] L. Li, Z. Ma, F. Bi, H. Li, W. Zhang, H. He, Sol-gel preparation and properties of Bi 4 Ti 3 O 12 photocatalyst supported on micrometer-sized quartz spheres, J. Adv. Oxid. Technol. 19 (2016) 310–316.
[27] I. Repository, Fabrication and photoelectrochemical studies of BiTiO pyrochlore thin lms by aerosol assisted chemical vapour deposition, Mater. Lett. 137 (2014) 214–217.
[28] G. Li, F. Zheng, Y. Tong, Controllable synthesis of Bi 2 Te 3 intermetallic compounds with hierarchical nanostructures via electrochemical deposition route, Cryst. Growth Des. 8 (2008) 1226–1232.
[29] B.L.W. Zhang, Y.J. Wang, H.Y. Cheng, W.Q. Yao, Y.F. Zhu, Synthesis of porous Bi2WO6 thin films as efficient visible-light-active photocatalysts, Adv. Mater. 21 (2009) 1286–1290.
[30] M. Ratova, G.T. West, P.J. Kelly, Photocatalytic visible-light active bismuth tungstate coatings deposited by reactive magnetron sputtering, Vacuum 115 (2015)

66–69.
[31] H.F. Schr, D. Puig, D. Barcel, Determination of phenolic compounds in water and waste water, Trends Analyt. Chem. 15 (1996) 362–375.
[32] F. Gnudi, Technical note phenolic compounds in surface water, Wat. Res 33 (1999) 3213–3219.
[33] N.A. Boroujeni, M. Hassanshahian, S. Mohammad, R. Khoshrou, Isolation and characterization of phenol degrading bacteria from Persian Gulf, Int. J. Adv. Biol. Biomed. Res. 2 (2014) 408–416.
[34] A.T. Lebedev, O.V. Poliakova, I.V. Dianova, Contamination of the Caspian Sea ecosystem with organic pollutants, Trans. Ecol. Environ. 49 (2001) 291–297.
[35] A.T. Lebedev, V. Poliakova, M.N. Repina, N.S. Sokolov, Contamination of the Caspian Sea ecosystem with organic pollutants, Trans. Ecol. Environ. 65 (2003) 115–124.
[36] T. Soltani, M.H. Entezari, Solar-Fenton catalytic degradation of phenolic compounds by impure bismuth ferrite nanoparticles synthesized via ultrasound, Chem. Eng. J. 251 (2014) 207–216.
[37] K. Wang, Y. Hsieh, M. Chou, C. Chang, Photocatalytic degradation of 2-chloro and 2-nitrophenol by titanium dioxide suspensions in aqueous solution, Appl. Catal. B 21 (1999) 3–10.
[38] S. Qourzal, N. Barka, M. Belmouden, A. Abaamrane, S. Alahiane, M. Elouardi, A. Assabbane, Y. Ait-Ichou, Heterogeneous photocatalytic degradation of 4-nitrophenol on suspended titania surface in a dynamic photoreactor, Fresenius Environ. Bull. 21 (2012) 1972–1981.
[39] O.J. Hao, M.H. Kim, E.A. Seagren, H. Kim, Kinetics of phenol and chlorophenol utilization by Acinetobacter species, Chemosphere. 46 (2002) 797–807.
[40] H. Al-Ekabi, N. Serpone, Kinetic Studies in Heterogeneous Photocatalysis. 2. Ti02-mediated degradation of 4-chlorophenol alone and in a three-component mixture of 4-Chlorophenol, 2,4-Dichlorophenol, and 2,4,5-Trichlorophenol in air-equilibrated, Langmuir 5 (1989) 250–255.
[41] M.F. Trentacoste, Enhanced night visibility series: phases ii and iii-characterization of experimental vision enhancement systems, XVII XVII (2005).
[42] Y. Ma, Zh. Tie, M. Zhou, N. Wang, Xia Cao, Y. Xie, Accurate determination of low-level chemical oxygen demand using a multistep chemical oxidation digestion process for treating drinking water samples, Anal. Methods 1 (2016) 2–6.
[43] R.L. Frost, M. Weier, Raman microscopy of selected autunite minerals, Spectrochim. Acta A 60 (2004) 1853–1859.
[44] H.C. Hamaker, Formation of a deposit by ELECTROPHORESIS, Trans. Faraday Soc 35 (1975) 279–287.
[45] B. Aksakal, A.R. Boccaccini, Electrophoretic deposition of selenium, Mater. Lett. 76 (2012) 177–180.
[46] K.T. Sullivan, J.D. Kuntz, A.E. Gash, Electrophoretic deposition and mechanistic studies of nano-Al/CuO thermites, J. Appl. Phys. 112 (2012) 1–11.
[47] Y. Zou, W. Zhou, J. Sunarso, F. Liang, Z. Shao, Electrophoretic deposition of YSZ thin-film electrolyte for SOFCs utilizing electrostatic-steric stabilized suspensions obtained via high energy ball milling, Int. J. Hydrogen Energy 36 (2011) 9195–9204.
[48] N. Koura, T. Tsukamoto, T. HiromasaShoji, Hotta, Preparation of various oxide films by an electrophoretic deposition method: a study of the mechanism, J. Appl. Phys. 34 (1995) 1643–1647.
[49] P. Sarkar, P.S. Nicholson, Electrophoretic deposition kinetic mechanism for ceramics, J. Am. Ceram. Soc. 79 (1996) 1987–2002.
[50] M. Choi, J. Lim, W. Choi, W. Kim, K. Yong, investigating the unrevealed photocatalytic activity and stability of nanostructured brookite TiO2 film as an environmental photocatalyst, ACS Appl. Mater. Interfaces 9 (2017) 16252–16260.
[51] M. Ratova, P. Kelly, G. West, X. Xia, Y. Gao, Deposition of visible light active photocatalytic bismuth molybdate thin films by reactive magnetron sputtering, Materials 9 (2016) 67–80.
[52] X. Guo, X. Li, C. Lai, W. Li, D. Zhang, Z. Xiong, Cathodic electrophoretic deposition of bismuth oxide (Bi2O3) coatings and their photocatalytic activities, Appl. Surf. Sci. 331 (2015) 455–462.
[53] M. Janczarek, A. Zielińska-Jurek, I. Markowska, J. Hupka, Transparent thin films of Cu–TiO_2 with visible light photocatalytic activity, Photochem. Photobiol. Sci. 14 (2015) 591–596.
[54] Y. Lu, L. Hao, K. Toh, H. Yoshida, Fabrication of TiO2/Cu composite photocatalyst thin film by 2-step mechanical coating technique and its photocatalytic activity, Adv. Mater. Res. 415–417 (2011) 1942–1948.
[55] A.L.M. Franco, G. Zambrano, M.E. Gómez, E. Camps, L. Escobar-Alarcón, Photocatalytic activity of nitrogen-doped and undoped titanium dioxide sputtered thin films, Superf. y Vacio. 25 (2012) 161–165.
[56] A. Eshaghi, A. Eshaghi, Photocatalytic properties of Cr doped TiO 2 – SiO 2 nanostructure thin film, Ceramics – Silikáty 56 (2012) 135–138.
[57] C. Lin, Y. Song, L. Cao, S. Chen, TiO_2 nanotubes/ZnO/CdS ternary nanocomposites: preparation, characterization and photocatalysis, J. Chinese Adv. Mater. Soc. 1 (2013) 188–199.
[58] S.A. Siuleiman, D.V. Raichev, A.S. Bojinova, D.T. Dimitrov, K.I. Papazova, Nanosized composite ZnO/TiO 2 thin films for photocatalytic applications, Bulg. Chem. Commun. 45 (2013) 649–654.
[59] J. Rashid, M.A. Barakat, N. Salah, S.S. Habib, Journal of Industrial and Engineering Chemistry ZnO-nanoparticles thin films synthesized by RF sputtering for photocatalytic degradation of 2-chlorophenol in synthetic wastewater, J. Ind. Eng. Chem. 23 (2015) 134–139.
[60] M. Duta, D. Perniu, A. Duta, Photocatalytic zinc oxide thin films obtained by surfactant assisted spray pyrolysis deposition, Appl. Surf. Sci. 306 (2014) 80–88.
[61] D. Komaraiah, E. Radha, Y. Vijayakumar, J. Sivakumar, M.V.R. Reddy, R. Sayanna, Optical, Structural and Morphological Properties of Photocatalytic ZnO Thin Films Deposited by Pray Pyrolysis Technique, Mod. Res. Catal. 05 (2016) 130–146.
[62] L. Cheng, L. Liu, R. Li, J. Zhang, Liquid Phase Deposition of α-Fe_2O_3/ZnO Heterojunction Film with Enhanced Visible-Light Photoelectrocatalytic Activity for Pollutant Removal, J. Electrochem. Soc. 164 (2017) H726–H733.